The DOI for this manuscript is
DOI:10.2151/jmsj.2023-007
J-STAGE Advance published date: November 14th, 2022

Atmospheric circulations associated with sea-ice reduction events in the Okhotsk Sea

Youichi KAMAE*, Hiroaki UEDA, Tomoshige INOUE

Faculty of Life and Environmental Sciences, University of Tsukuba, Tsukuba, Japan

and

Humio MITSUDERA

Pan Okhotsk Research Center, Institute of Low Temperature Science, Hokkaido University, Sapporo, Japan

----

*) Corresponding author: Youichi Kamae, Faculty of Life and Environmental Sciences, University of Tsukuba, 1-1-1 Tennoudai, Tsukuba, Ibaraki 305-8572, JAPAN

Email: kamae.yoichi.fw@u.tsukuba.ac.jp

Tel: +81-29-853-5878

Fax: +81-29-853-6709

Abstract

Wintertime sea ice cover in the Okhotsk Sea (OS) exhibits strong interaction with the atmosphere over the Far East and the North Pacific. Previous studies identified that interannual variability of sea ice cover in the OS is associated with large-scale atmospheric circulations. However, the atmospheric processes responsible for rapid changes in sea ice cover in the OS on subweekly-weekly timescales remain unclear. Here, we investigate the atmospheric circulations that contribute to rapid reduction events of OS sea ice concentration (OSSIC) using daily high-resolution ocean reanalysis data. In total, we detected 21 rapid reduction events of OSSIC during 1993–2019. The reduction events shared common features in terms of atmospheric circulation, i.e., a developing extratropical cyclone over the southern OS and anomalous high pressure over the northern Bering Sea with strong surface southeasterly winds between the two. The strong southeasterlies, which blow in the opposite direction to the surface westerlies that regulate the seasonal development of sea ice cover, result in the rapid reduction of OSSIC. Substantial reduction in sea ice occurs in the northern and central OS owing to sea ice advection and sea ice melt associated with the easterly winds. The eastward-moving extratropical cyclone contributes both to rapid reduction of OSSIC and to reduction of sea level pressure over the northern North Pacific, resulting in a lagged relationship between OSSIC and the Aleutian Low.

Keywords Okhotsk Sea, sea ice, extratropical cyclone

1. Introduction

The Okhotsk Sea (OS), which is located east of Siberia, is well known as one of the southernmost areas (44°–62°N) with a large fraction of seasonal sea ice cover (between November and June). More than half (50%–90%) of the OS is covered by sea ice during late February to early March (Ohshima et al. 2006). Spatial distributions of wintertime sea-ice cover and seasonal retreat/melt are consequences of multiple factors that include wind stress, ocean currents, and river discharge (e.g., Kimura and Wakatsuchi 1999; Ogi et al. 2001; Ohshima et al. 2005; Simizu et al. 2014). Seasonal retreat/melt and interannual variability of sea ice in the OS lead both to large variations in the heat budget at the sea surface and to atmosphere–sea-ice–ocean interactions (Ohshima et al. 2003, 2006; Nihashi et al. 2011). Through substantial variations in surface heat flux, sea ice variability also leads to atmospheric teleconnections that include modulations of large-scale circulation patterns over Alaska and North America via Rossby wave propagation (Honda et al. 1999; Williams et al. 2021).

Large interannual variability in sea ice concentration~~s~~ (SIC) in the OS (hereafter, OSSIC) has attracted considerable attention from the perspective of the effects of large-scale atmospheric circulations. Previous studies found statistical connections of OSSIC interannual variability with the East Asian winter monsoon, Aleutian Low, Arctic Oscillation and North Atlantic Oscillation (Parkinson 1990; Tachibana et al. 1996; Yamazaki 2000; Liu et al. 2007; Yang et al. 2011; Toyoda et al. 2022). Toyoda et al. (2022) compared the interannual variability of yearly maximum areal coverage of OSSIC and large-scale climate indices and found that the North Pacific Index (NPI), which is an index that reflects the strength of the Aleutian Low, showed significant negative correlation (i.e., a stronger Aleutian Low tends to coincide with larger OSSIC), at least since the 1980s. Additionally, Fang and Wallace (1998) and a number of more recent studies (Yamazaki 2000; Sasaki et al. 2007; Linkin and Nigam 2008; Yang et al. 2011) highlighted the significant relationship between the Western Pacific Pattern (Wallace and Gutzler 1981) and the interannual variability of OSSIC through sea ice drift (dynamic effect) or sea ice melt due to warm advection (thermodynamic effect).

The previous studies examined the month-to-month features or interannual variability of the seasonal- mean OSSIC (Fang and Wallace 1998; Yamazaki 2000; Liu et al. 2007; Sasaki et al. 2007; Ukita et al. 2007; Yang et al. 2011). Using data with higher temporal resolution, Strong et al. (2009) identified variability of sea ice in both the Arctic Sea and the Greenland Sea on a weekly timescale that was associated with North Atlantic Oscillation atmospheric forcing. Matthewman and Magnusdottir (2011) revealed a statistical relationship between the Western Pacific Pattern and SIC in the Bering Sea on a weekly timescale. Recently, Toyoda et al. (2022) examined the year-to-year variations in the dates of first appearance and final disappearance of sea ice at the Japan Meteorological Agency observatories located along the Hokkaido coast, and they found that they are related statistically to the Aleutian Low. Such studies motivated us to examine the relationship between day-to-day variations in the spatial patterns of OSSIC and the transient atmospheric disturbances over the OS.

Here, we investigate the day-to-day variability of SIC in the OS and the associated atmospheric circulations. Using daily SIC data and atmospheric reanalysis data, we examine the relationship between the two with particular emphasis on SIC reduction events because they represent striking features that are not well understood. Section 2 describes the observations and reanalysis data used for the investigation. Section 3 introduces a typical SIC reduction event and the associated atmospheric circulation pattern. Results of composite analyses of similar SIC reduction events are also examined. Finally, Section 4 presents a summary and discussion.

2. Data and Method

We used daily outputs of the Copernicus Marine Environment Monitoring Service global eddy-resolving physical ocean reanalysis GLORYS12V1 for 1993–2019 (Lellouche et al. 2021). The NEMO global ocean model (Madec et al. 2008) with horizontal resolution of 1/12° and 50 vertical levels was driven at the surface by the atmospheric reanalysis of the European Centre for Medium-Range Weather Forecasts (ERA-Interim; Dee et al. 2011). A reduced-order Kalman filter was used for assimilation of state-of-the-art observations (along-track altimeter data, sea surface temperature (SST), and SIC from satellite observations, and in situ temperature and salinity vertical profiles). We used daily mean fields of SIC in this dataset. We confirmed that the results of the SIC analyses were generally consistent with those obtained from the Optimum Interpolation Sea Surface temperature (OISST) version 2 (Reynolds et al. 2007; see Supplement 1). Figure 1 shows the SIC climatology of the OS averaged between January and March. Areas of high concentration of sea ice are found around Shantarskiy Bay and the east coast of Sakhalin Island. In this study, we obtained OSSIC by averaging the SIC in the region of 44°–62°N, 135°–157°E (Fig. 1). To compare regional SIC variability, we also calculated the area-averaged SIC in the northern and central OS (black shape in Fig. 1) and in the Sakhalin and Hokkaido coastal region (red shape in Fig. 1).

Fig. 1

We used the 6-hourly outputs from the Japanese 55-year Reanalysis (JRA-55; Kobayashi et al. 2015) to examine the relationship between OSSIC variability and the atmospheric fields. Geopotential height at the 500 hPa level, sea level pressure (SLP), and horizontal wind at 925 hPa were used in this study. We calculated daily mean fields by averaging the 6-hourly atmospheric fields. To investigate the zonal wind in the OS, we calculated the area-averaged 925-hPa zonal wind over the OS (hereafter, UOS) region (blue dashed rectangle in Fig. 1).

3. Results

3.1 Sea ice reduction event of early February 2005

Figure 2 shows time series of OSSIC in individual years from 1993/94 to 2018/19. Sea ice

Fig. 2

in the OS generally begins to form in Shantarskiy Bay in late November, peaks in February–March, and then disappears by May or June (Ohshima et al. 2006). The seasonal peak of OSSIC (35% in terms of climatology) shows large interannual variability, as examined in many previous related studies (Fang and Wallace 1998; Yamazaki 2000; Liu et al. 2007; Sasaki et al. 2007; Ukita et al. 2007; Yang et al. 2011). During the period of OSSIC growth (before February or March), OSSIC is sometimes reduced substantially on subweekly-to-weekly timescales. As an example of such a reduction event (RE), OSSIC of 28% was reduced to 23% from January 29 to February 8, 2005 (Fig. 2). Figure 3a shows SIC in the OS during this event. It can be seen that SIC reduced substantially in the northern and central OS (47°–58°N, 143°–152°E) but increased along the Sakhalin and Hokkaido coastal region (44°–54°N, 142°–145°E).

Fig. 3

We found an important contribution of atmospheric forcing to OSSIC reduction. Figure 4 shows the SLP and geopotential height fields on January 30 and February 2, 2005. On January 30, a trough and a ridge are found over northeastern China to Japan and over the northwestern North Pacific Ocean (160°E) to the OS, respectively (Fig. 4a). At the surface, an extratropical cyclone over northern Japan moved eastward to the southern OS (Fig. 4c). On February 2, the trough moved over the northwestern North Pacific Ocean (Fig. 4b). The developed extratropical cyclone at the surface moved eastward and merged with the area of low pressure over the North Pacific, resulting in a west-high east-low SLP pattern over East Asia (Fig. 4d).

Fig. 4

The extratropical cyclone induced a strong surface wind over the OS. The densely packed isobars over the OS (Fig. 4c, d) suggest strong southeasterly and easterly surface winds over the central and southern OS on January 30, and easterly and northeasterly surface winds over the OS on February 2. Such strong surface winds potentially affected the surface ocean current (Fig. 3b; also see Sect. 3.3) and sea ice distribution in the OS (Kimura and Wakatsuchi 2000; Simuzu et al. 2014). Additionally, because of the surface temperature gradient over the northwestern North Pacific and the OS (Supplement 2), the easterlies also facilitated sea ice melt owing to warm air advection (see Sect. 3.3). In the next subsection, we consider similar REs and identify common features in the atmospheric circulation fields.

3.2 Composite analyses

Figure 5 shows OSSIC time series in individual years from December 1 to March 16. In addition to the large interannual variability in the seasonal-mean OSSIC (maximum in 2000/01 and minimum in 2014/15), intraseasonal variability of OSSIC (including the RE in early February 2005) can also be found. In this study, we determined the time tendency of OSSIC (ΔOSSIC) as follows: Fig. 5

$$\Delta \mathrm{OSSIC}(T) = (\mathrm{OSSIC}(T+1) - \mathrm{OSSIC}(T-1)) / 2, \quad (1)$$

where OSSIC(T) represents OSSIC on day T. Generally, ΔOSSIC tends to be positive from early December to mid-February (reflecting the seasonal increase in SIC) but it sometimes takes a negative value. In this study, we determined a period as an RE if the period satisfied the following conditions: (1) it occurred between December 1 and February 15; (2) it occurred before OSSIC reached its seasonal peak (e.g., before February 7 in 2017); and (3) the period of negative ΔOSSIC persisted for at least 4 days. We used requirements (1) and (2) to restrict the obtained REs to events that occurred during the period of sea ice growth in the given year. We confirmed that rapid reductions of sea ice over the southern OS due to spring storm-induced sharp temperature rises ("Haru-Ichiban"; Nishii et al. 2009) were included if we did not limit the target periods using the above requirements (1) and (2). The relationship between storm-induced southerly warm advection and sea ice melt in the OS during late winter to early spring is worthy of examination in future studies.

Table 1 summarizes the REs detected between the winters of 1993/94 and 2018/19. In total, we detected 21 REs with duration in the range of 4–11 days. It should be noted that the period between January 22 and February 1, 2003 included 2 days with positive (albeit small) ΔOSSIC values but it was still considered an RE. Comparison of the REs and UOS (see Sect. 2; Fig. 5) reveals that all 21 REs were accompanied with easterly winds at the 925 hPa level over the OS (negative UOS) despite the northwesterly climatological winds (Kimura and Wakatsuchi 2004). Note that not all the easterly events, especially in December (e.g., December 13–19, 1999 and December 10–17, 2013), were accompanied by REs. In early winter, OSSIC itself tends to be limited; therefore, its response to the atmospheric forcing should also be limited.

Table 1

Figure 6 shows a composite of the atmospheric circulation fields during the REs. As found

Fig. 6

in the RE of February 2005 (Fig. 4b), a meridional pair of positive and negative geopotential height anomalies northward of the OS and northern Japan is consistently found in the 21 REs. The statistically significant positive anomaly is elongated zonally (90°–170°E) and forms a strong meridional gradient toward the negative anomaly (20°–45°N, 125°–165°E). The SLP anomaly (Fig. 6b) also shows a meridional pattern (north-positive, south-negative). The negative SLP anomaly is found over the southern OS, northern Japan, and the northwestern North Pacific Ocean. The positive SLP anomaly is elongated zonally between Alaska and Siberia with its peak over the northern Bering Sea. The resultant strong SLP gradient over the OS suggests strong low-level southeasterlies and easterlies over the OS along the isobars. The strong surface easterlies blow in the direction opposite to that of the climatology (westerlies), resulting in the SIC reduction in the OS (Kimura and Wakatsuchi 1999; Linkin and Nigam 2008; Williams et al. 2021).

Figure 6a also shows SST anomalies in the Indian and Pacific Oceans during the REs. Although positive or negative SST anomalies are found in the composite analyses (e.g., cool SST over the eastern equatorial Pacific), no statistically significant anomaly at the 95% confidence level was found over the tropics. This weak relationship indicates that tropical SST forcing is not the dominant factor affecting the REs. However, SST over the Kuroshio extension region (35°–50°N, 140°E–170°W) does exhibit correlation with OSSIC, as suggested in Fang and Wallace (1998).

3.3 Temporal evolutions

The negative SLP anomaly over the southern OS (Fig. 6b) corresponds to the eastward-moving extratropical cyclones (Fig. 4). Figure 7 shows the composite mean fields of SLP anomaly and low-level wind anomaly from day –4 to day +6 to examine the temporal evolutions of the atmospheric circulation fields associated with OSSIC reduction. Here, day 0 denotes the start of the RE. Figure 8 shows the spatial patterns of ΔOSSIC and the low-level wind over the OS. On day –4, with increasing OSSIC (Fig. 7a), no statistically significant anomaly is found in the atmospheric circulation field (Supplement 3). Figure 9 shows the time series of ΔOSSIC from day –15 to day +15. Because the REs detected in this study occurred during the period of sea ice growth, ΔOSSIC tends to have positive values, including statistically significant positive values from day –5 to day –3. On day –2, the surface high pressure anomaly over the Bering Sea becomes stronger and significant (Fig. 7b, Supplement 3). Furthermore, a statistically significant low pressure anomaly (reflecting the extratropical cyclones; Fig. 4c) is found over the Korean Peninsula and western Japan. The low pressure anomaly becomes stronger and moves eastward to the southern OS on day 0 (Fig. 7c). The strong pressure gradient between the high pressure anomaly over the Bering Sea and the low pressure anomaly results in the strong southeasterly anomaly over the OS (Fig. 7c). This southeasterly anomaly indicates a reversal of the wind direction from the climatological northwesterly winds (Kimura and Wakatsuchi 2004) over the central and southern OS (Fig. 8c), contributing to the remarkable

Fig. 7

Fig. 8

Fig. 9

OSSIC reduction.

Between day 0 and day +4, corresponding to the period of reduction of OSSIC, negative ΔOSSIC is found over the northern and central OS (Fig. 8c–e). On day +4, the center of the low pressure anomaly moves to the North Pacific (170°E) and the high pressure anomaly becomes stronger both over Siberia (120°E) and over the northern OS (170°E; Fig. 7e). The strong meridional pressure gradient over the North Pacific Ocean causes an easterly surface wind anomaly over the Bering Sea and the OS (Fig. 7e). On day +6, SIC reduction is weakened in the northern OS but is found in the central OS (Fig. 8f). Between day +4 and day +6, the low pressure extends across the North Pacific Ocean, indicating an intensified Aleutian Low (Fig. 7e, f). The SLP anomaly averaged over the region of the NPI (30°–65°N, 160°E–140°W; Trenberth and Hurrel 1994) becomes statistically significant with negative sign from day +5 to day +12 (Fig. 9a). The SST anomaly averaged over the Niño3.4 region (5°S–5°N, 170°–120°W) is consistently negative from day –15 to day +15 without statistical significance at the 95% confidence level.

In Fig. 9, negative ΔOSSIC can be found from day 0 to day +4. If we compare ΔOSSIC with its climatology, the negative ΔOSSIC anomaly (relative to its climatology) is statistically significant from day –1 to day +6 and it returns to the climatology on day +8. The period with a statistically significant negative anomaly of ΔOSSIC is also characterized by negative UOS (easterly wind at 925 hPa over the northern and central OS; statistically significant from day –1 to day +6; Figs. 8 and 9). The two time series are remarkably similar, suggesting a strong relationship between OSSIC and the low-level zonal wind on a subweekly timescale.

Regionally, we find a contrasting feature of the time tendency of SIC within the OS. In Fig. 9b, the time series of ΔSIC in the northern and central OS (see Fig. 1) resembles that of the entire OS, indicating that the reduction of SIC during an RE is dominant in the northern and central OS. This SIC reduction is accompanied by reduction in sea water salinity in the northern and central OS (green line in Fig. 9b). The statistically significant negative anomaly in salinity (relative to its climatology) from day –1 to day +3 suggests that sea ice melt contributes to the negative ΔSIC in this region. Sea ice melt was possibly caused by warm air advection induced by the easterly wind. Surface air over the eastern OS and the northwestern North Pacific Ocean is warmer than that over Siberia and the western OS (Supplement 2). Thus, reversal of the wind direction contributes to SIC reduction via the thermodynamic effect.

In contrast to the SIC reduction in the northern and central OS, ΔSIC in the Sakhalin and Hokkaido coastal region (47.6°–62.0°N, 142.3°–155.1°E) is positive with statistical significance between day –1 and day 0. The SIC increase in the Sakhalin and Hokkaido coastal region is also found in the RE of early February 2005 (Fig. 3). This inverse tendency between the two regions suggests an effect of sea ice advection and/or coastal sea ice production. The strong southeasterlies on day 0 weaken eastward expansion of sea ice, resulting in sea ice advection (Kimura and Wakatsuchi 2004) from the northern and central OS toward the Sakhalin coast (Figs. 3b and 8c). Between day –4 and day –2, northwesterly winds dominate over the Sakhalin coast (Fig. 8a, b) but they shift to northerly or northeasterly winds on day 0 (Fig. 8c). The northerly winds and associated southward advection result in SIC increase in the southern Sakhalin and Hokkaido coastal region (Figs. 3b and 8c).

The north-high south-low SLP pattern and associated easterly wind over the OS are sustained for a period of days to a week (Fig. 7a), suggesting reduction in sea ice production along the Sakhalin coast (Kimura and Wakatsuchi 2004). The results of this study suggest that eastward-moving extratropical cyclones over Japan have three important effects on SIC in the OS: (1) reduction in SIC in the northern and central OS due to warm air advection driven by easterly winds; (2) SIC reduction contributed by sea ice advection; and (3) temporary increase in sea ice along the Sakhalin coast. The third effect is not sustained because northeasterly winds also suppress sea ice production in this region.

4. Summary and discussion

Using daily SIC data, we investigated the meteorological processes responsible for the rapid reductions of OSSIC that occur in boreal winters. We found that surface easterly winds over the OS associated with eastward-moving extratropical cyclones made significant contributions to the REs detected during 1993–2019. The extratropical cyclones over the southern OS and anomalously high SLP over the Bering Sea produce strong southeasterly and easterly surface winds over the OS at the start and during the REs, respectively. All the REs occurred during the periods with reversal of the low-level wind direction, indicating the close relationship between the transient atmospheric eddies and the OSSIC. The easterlies result in reduction of SIC in the northern and central OS, possibly owing to sea ice advection and sea ice melt associated with warm air advection. Sea ice advection also contributes to the increase in SIC along the Sakhalin coast. The NPI becomes negative after the start of the REs with a 3-day lag because of the extratropical cyclone moving eastward from the southern OS to the North Pacific Ocean. Here, we only suggest possible contributions to regional SIC variability by sea ice melt and sea ice advection associated with the easterly winds. Further research based on ocean–sea-ice–atmosphere coupled model simulations is needed for quantitative evaluation of the dynamic/thermodynamic contributions.

The subseasonal features of OSSIC and associated atmospheric circulations identified in this study are potentially important in terms of the interannual variability of the seasonal mean OSSIC. Liu et al. (2007) identified that the seasonal mean negative SLP anomaly over the OS and the North Pacific Ocean tends to be observed in years with light SIC in the OS and the Bering Sea (Fig. 3b in Liu et al. 2007). Yang et al. (2011) showed that a weaker Aleutian Low and lower SLP over the southern OS are found during years with less OSSIC (Fig. 5a in Yang et al. 2011). These SLP patterns are partly consistent with the composite patterns during the REs detected in the current study (Fig. 6b). However, the seasonal mean anomaly of the atmospheric circulation fields associated with the interannual variability of OSSIC identified in previous studies should also include the effect of the OSSIC perturbation to the atmosphere (Honda et al. 1999), which exhibits a similar SLP pattern (low SLP anomaly over the OS and high SLP anomaly over the Bering Sea during periods with low OSSIC) to that in this study. The results of the current study are potentially helpful for illuminating the importance of subseasonal processes on the interannual variability of OSSIC.

Supplement

Supplement 1 provides SIC in the Okhotsk Sea for the example case of early February 2005 obtained from OISST V2. Supplement 2 shows the climatology in surface air temperature in the OS. Supplement 3 shows the statistical significance of the SLP anomalies shown in Fig. 7.

Acknowledgments

We appreciate the helpful comments and suggestions from S. Minobe and M. Kuramochi. This research was supported by the Environment Research and Technology Development Fund (JPMEERF20214002) of the Environmental Restoration and Conservation Agency of Japan, and JSPS KAKENHI Grand Number 19H05703. We are grateful to M. Honda and the two anonymous reviewers for their constructive comments. We thank J. Buxton, MSc, from Edanz (https://jp.edanz.com/ac) for editing a draft of this manuscript.

Data availability statements

JRA-55 is available at http://search.diasjp.net/en/dataset/JRA55. GLORYS12V1 is available at https://doi.org/10.48670/moi-00021.

References

Dee, D. P., S. M. Uppala, A. J. Simmons, et al., 2011: The ERA-Interim reanalysis: configuration and performance of the data assimilation system. Quart. J. Royal Meteor. Soc., **137**, 553–597.

Fang, Z., and J. M. Wallace, 1998: North-Pacific sea ice and Kuroshio SST variability and its relation to the winter monsoon. Polar Meteor. Glaciol., **12**, 58–67.

Honda, M., K. Yamazaki, H. Nakamura, and K. Takeuchi, 1999: Dynamic and thermodynamic characteristics of atmospheric response to anomalous sea-ice extent in the Sea of Okhotsk. J. Climate, **12**, 3347–3358.

Kimura, N., and M. Wakatsuchi, 1999: Processes controlling the advance and retreat of sea ice in the Sea of Okhotsk. J. Geophys. Res., **104**, C5, 11137–11150.

Kimura, N., M. Wakatsuchi, 2000: Relationship between sea-ice motion and geostrophic wind in the Northern Hemisphere. Geophy. Res. Lett., **27**, 3735–3738.

Kimura, N., and M. Wakatsuchi, 2004: Increase and decrease of sea ice area in the Sea of Okhotsk: Ice production in coastal polynyas and dynamic thickening in convergence zones. J. Geophys. Res., **109**, C09S03, doi:10.1029/2003JC001901.

Kobayashi, S., Y. Ota, Y. Harada, A. Ebita, M. Moriya, H. Onda, K. Onogi, H. Kamahori, C.

Kobayashi, H. Endo, K. Miyaoka, and K. Takahashi, 2015: The JRA-55 Reanalysis: General specifications and basic characteristics. J. Meteor. Soc. Japan, **93**, 5–48.

Lellouche, J.-M., E. Greiner, R. Bourdallé-Badie, G. Garric, A. Melet, M. Drévillon, et al. 2021: The Copernicus global 1/12° oceanic and sea ice GLORYS12 reanalysis. Front. Earth Sci., **9**, 698876.

Linkin, M. E., and S. Nigam, 2008: The North Pacific Oscillation–West Pacific teleconnection pattern: Mature-phase structure and winter impacts. J. Climate, **21**, 1979–1997.

Liu, J., Z. Zhang, R. M. Horton, C. Wang, and X. Ren, 2007: Variability of North Pacific sea ice and East Asia–North Pacific winter climate. J. Climate, **20**, 1991–2001.

Madec, G., and the NEMO team, 2008: NEMO ocean engine. Note du Pôle de modélisation, Institut Pierre-Simon Laplace (IPSL), France,1288–1619.

Matthewman, N. J., and G. Magnusdottir, 2011: Observed interaction between Pacific sea ice and the Western Pacific pattern on intraseasonal time scales. J. Climate, **24**, 5031–5042.

Nihashi, S., K. I. Ohshima, and H. Nakasato, 2011: Sea-ice retreat in the Sea of Okhotsk and the ice–ocean albedo feedback effect on it. J. Oceanogr., **67**, 551–562.

Nishii, K., T. Miyasaka, Y. Kosaka, and H. Nakamura, 2009: Reproducibility and future projection of the midwinter storm-track activity over the Far East in the CMIP3 climate models in relation to ‘‘Haru-Ichiban’’ over Japan. J. Meteor. Soc. Japan, **87**, 581–588.

Ogi, M., Y. Tachibana, F. Nishio, and M. A. Danchenkov, 2001: Does the fresh water supply from the Amur River flowing into the Sea of Okhotsk affect sea ice formation? J. Meteor. Soc. Japan, **79**, 123–129.

Ohshima, K. I., T. Watanabe, and S. Nihashi, 2003: Surface Heat Budget of the Sea of Okhotsk during 1987–2001 and the Role of Sea Ice on it. J. Meteor. Soc. Japan, **81**, 653–677.

Ohshima, K. I., S.C. Riser, and M. Wakatsuchi, 2005: Mixed layer evolution in the Sea of Okhotsk observed with profiling floats and its relation to sea ice formation. Geophys. Res. Lett., **32**, L06607, doi:10.1029/2004GL021823.

Ohshima, K. I., S. Nihashi, E. Hashiya, and T. Watanabe, 2006: Interannual variability of sea ice area in the Sea of Okhotsk: Importance of surface heat flux in fall. J. Meteor. Soc. Japan, **84**, 907–919.

Parkinson, C. L., 1990: The impact of the Siberian high and Aleutian low on the sea-ice cover of the Sea of Okhotsk. Ann. Glaciol., **14**, 226–229.

Reynolds, R. W., T. M. Smith, C. Liu, D. B. Chelton, K. S. Casey, and M. G. Schlax, 2007: Daily high-resolution-blended analyses for sea surface temperature. J. Climate, **20**, 5473–5496.

Sasaki, Y. N., Y. Katagiri, S. Minobe, and I. G. Rigor, 2007: Autumn atmospheric preconditioning for interannual variability of wintertime sea-ice in the Okhotsk Sea. J. Oceanogr., **63**, 255–265.

Simizu, D., K. I. Ohshima, J. Ono, Y. Fukamachi, and G. Mizuta, 2014: What drives the southward drift of sea ice in the Sea of Okhotsk? Prog. Oceanogr., **126**, 33–43.

Strong, C., G. Magnusdottir, and H. Stern, 2009: Observed feedback between winter sea ice and the North Atlantic Oscillation. J. Climate, **22**, 6021–6032.

Tachibana, Y., M. Honda, and K. Takeuchi, 1996: The abrupt decrease of the sea ice over the southern part of the Sea of Okhotsk in 1989 and its relation to the recent weakening of the Aleutian Low. J. Meteor. Soc. Japan, **74**, 579–584.

Toyoda, T., Y. Kitamura, R. Okada, K. Matsumura, K. K. Komatsu, K. Sakamoto, L. S. Urakawa, and H. Nakano, 2022: Sea ice variability along the Okhotsk coast of Hokkaido based on long-term JMA meteorological observatory data. Okhotsk Sea Polar Oceans Res., **6**, 27–35.

Trenberth, K. E., and J. W. Hurrell, 1994: Decadal atmosphere-ocean variations in the Pacific. Climate Dyn., **9**, 303–319.

Ukita, J., M. Honda, H. Nakamura, Y. Tachibana, D. J. Cavalieri, C. L. Parkinson, H. Koide, and K. Yamamoto, 2007: Northern Hemisphere sea ice variability: lag structure and its implications. Tellus, **59A**, 261–272.

Wallace, J. M., and D. S. Gutzler, 1981: Teleconnections in the geopotential height field during the Northern Hemisphere winter. Mon. Wea. Rev., **109**, 784–812.

Williams, M. Z., M. Gervais, and C. E. Forest, 2021: Causes and impacts of sea ice variability in the sea of Okhotsk using CESM-LE. Climate Dyn., **56**, 2007–2021.

Yamazaki, K., 2000: Interaction between the wintertime atmospheric circulation and the variation in the sea ice extent of the Sea of Okhotsk. Seppyo, **62**, 345–354 (in Japanese with English abstract).

Yang, X.-Y., J. Hu, J. Wang, and D. Wang, 2011: Linkage between winter air temperature over the subtropical Western Pacific and the ice extent anomaly in the Sea of Okhotsk. J. Oceanogr., **67**, 197–208.

List of Tables

List of Figures

Fig. 4 Geopotential height at 500 hPa (Z500; m) and sea level pressure (SLP; hPa) in the example case of early February 2005. (a) Contours indicate Z500 at 00 UTC on January 30 and (b) at 18 UTC on February 2, 2005. Shading represents Z500 anomaly relative to its climatology (1991–2020). (c) Contours and shading indicate SLP at 00 UTC on January 30, and (d) at 18 UTC on February 2, 2005.

Fig. 5 Time series of OSSIC and UOS between December 1 and March 16 in 26 winters (from 1993/94 to 2018/19). The horizontal axis ranges for the leap years (1996, 2000, 2004, 2008, 2012, and 2016) are from December 1 to March 15. Gray lines indicate OSSIC (%). Red and blue shading represents positive (westerly) and negative (easterly) UOS (m s^{-1}), respectively, determined as 925 hPa zonal wind averaged over 47.6°–59.0°N, 142.3°–155.1°E (Fig. 1). Shading in light magenta indicates sea-ice reduction events (REs).

Fig. 6 Composite Z500, SLP, and SIC in the Okhotsk Sea during periods of REs. (a) Red and blue contours indicate Z500 anomaly (±10, 20, 30, 40 and 50 m). Light blue-light red shading indicates sea surface temperature (SST; K) anomaly based on OISST version 2 (Reynolds et al. 2007). Blue-cyan shading in (a) and (b) indicates SIC in the Okhotsk Sea (%). (b) Red and blue contours indicate SLP anomaly (±0.5, 1.0, 1.5, 2.0, and 2.5 hPa). Vectors indicate horizontal wind anomaly (m s^{-1}) at 925 hPa. Stipples indicate areas with 95% statistical confidence of (a) the Z500 anomaly and (b) the SLP anomaly.

Fig. 7 Composite maps of SLP anomaly and horizontal wind anomaly at 925 hPa at (a) 4 days before the start of the REs (day –4), (b) day –2, (c) at the start (day 0), (d) 2 days after the start of REs (day +2), (e) day +4, and (f) day +6. Red (blue) contours indicate positive (negative) SLP anomaly (±0.5, 1.0, 1.5, 2.0, and 2.5 hPa). Vectors indicate horizontal wind anomaly (m s^{-1}) at 925 hPa.

Fig. 8 Similar to Fig. 7, but composite maps of horizontal wind at 925 hPa over the Okhotsk Sea region. Shading indicates time tendency of SIC (% day^{-1}) in the Okhotsk Sea. Stipples indicate areas with 95% statistical confidence of the time tendency of SIC.

Fig. 9 Lagged composite between day –15 and day +15. (a) Black line indicates time tendency of OSSIC (ΔOSSIC, % day^{-1}). Gray dotted line indicates climatology of ΔOSSIC. Blue line represents UOS (m s^{-1}). Green line indicates SST anomaly over the Niño3.4 region (5°S–5°N, 170°–120°W; K). Brown line indicates SLP anomaly over the North Pacific Index region (30°–65°N, 160°E–140°W; hPa). Thick lines indicate >95% confidence levels. Black thick line indicates >95% confidence levels of ΔOSSIC anomaly relative to its climatology (black line minus gray dotted line). (b) Black and magenta lines indicate time tendency of SIC in the Sakhalin and Hokkaido coastal region (43.5°–53.2°N, 142.3°–144.4°E) and the northern and central OS region (47.6°–62.0°N, 142.3°–155.1°E), respectively (Fig. 1). Green line indicates time tendency of sea surface salinity (PSU) in the northern and central OS region. Thick lines indicate >95% confidence levels of ΔSIC anomaly relative to the climatology (dotted lines).

Table. 1 Detected reduction events (REs) in Okhotsk Sea (OS) sea ice concentration (OSSIC). The case of January 22 to February 1, 2003 includes the period of January 26–27 with positive ΔOSSIC (Eq. (1)).

January 25–31, 1995
February 1–4, 1996
January 1–4, 1997
January 21–31, 1997
January 7–11, 1999
December 31, 2001 – January 5, 2002
February 7–12, 2002
January 22 – February 1, 2003
January 8–13, 2005
January 30 – February 7, 2005
January 19–24, 2006
December 26–31, 2008
February 5–8, 2010
December 23–28, 2010
January 14–17, 2011
January 24–27, 2012
January 17–20, 2013
January 10–15, 2017
December 25, 2017 – January 1, 2018
January 24–28, 2018
January 21–24, 2019

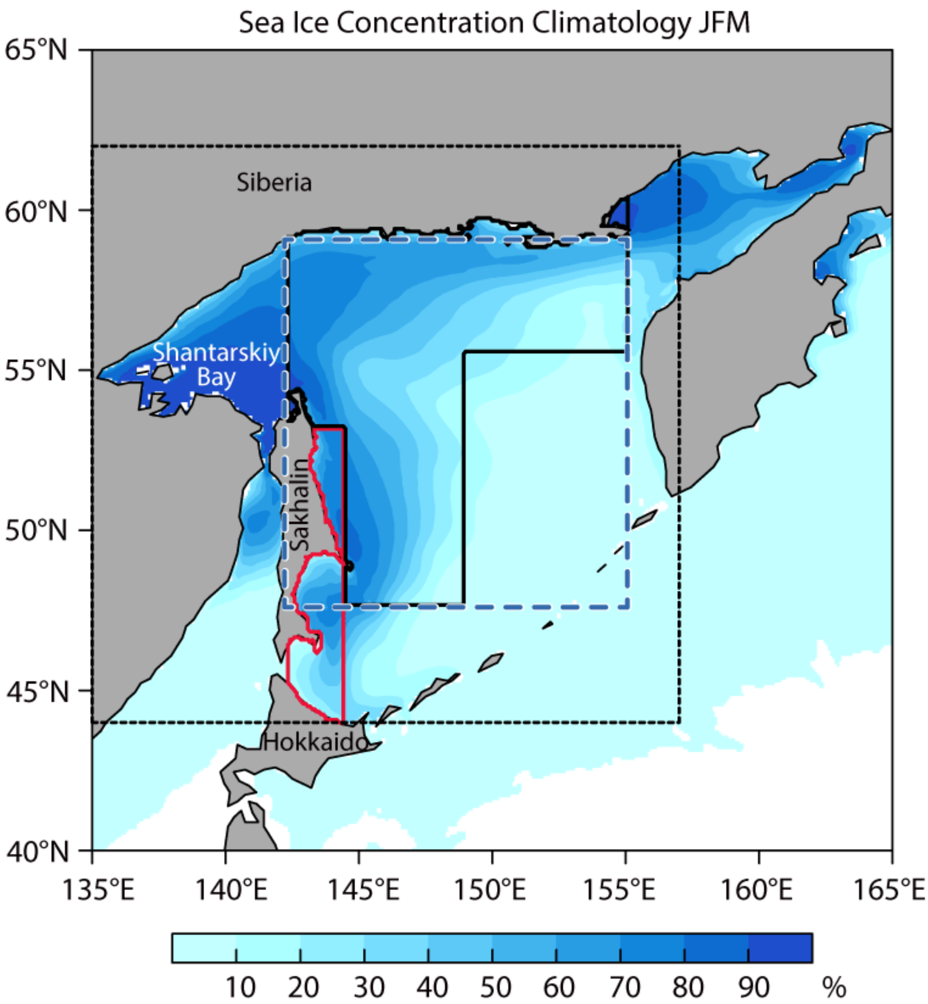

Fig. 1 Climatology of sea ice concentration (SIC; %) in the Okhotsk Sea (OS). SIC is averaged for 1993–2019 during January, February, and March. Black dashed rectangle indicates the region (44°–62°N, 135°–157°E) used for calculation of OSSIC. Red and black solid shapes indicate the Sakhalin and Hokkaido coastal region (44.0°–53.2°N, 142.3°–144.4°E) and the northern and central Okhotsk Sea region (47.6°–62.0°N, 142.3°–155.1°E), respectively. Blue dashed rectangle indicates the region (47.6°–59.0°N, 142.3°–155.1°E) used for calculation of the zonal wind over the Okhotsk Sea (UOS).

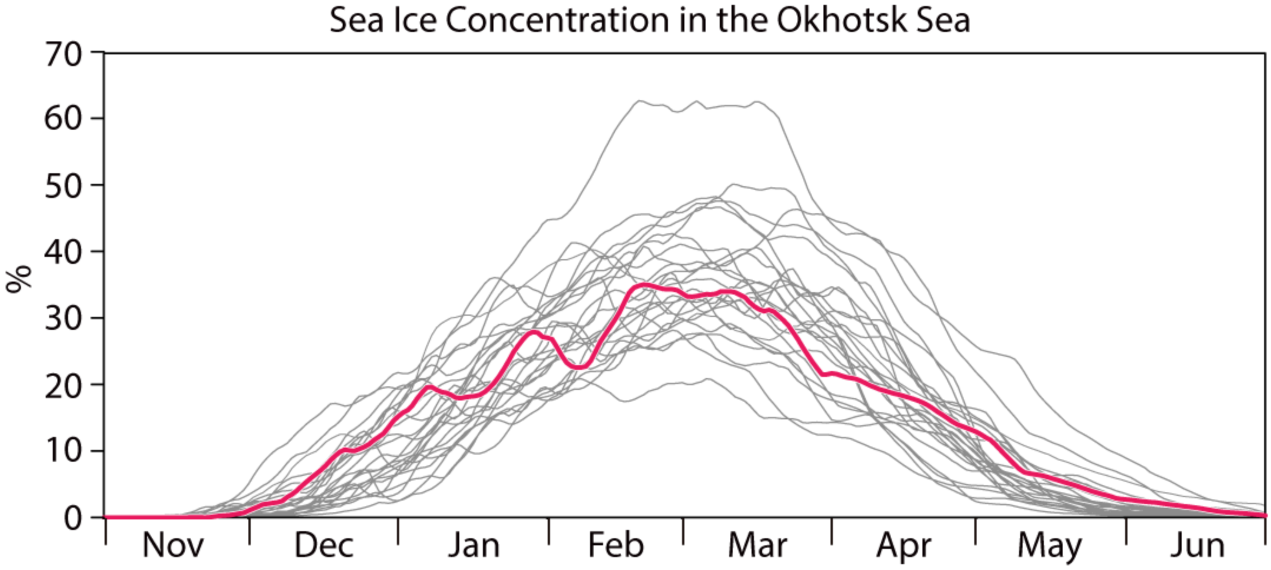

Fig. 2 Time series of OSSIC (%) between November 1 to June 30 in each year (1993/94–2018/19). Magenta line indicates OSSIC between November 1, 2004 and June 30, 2005.

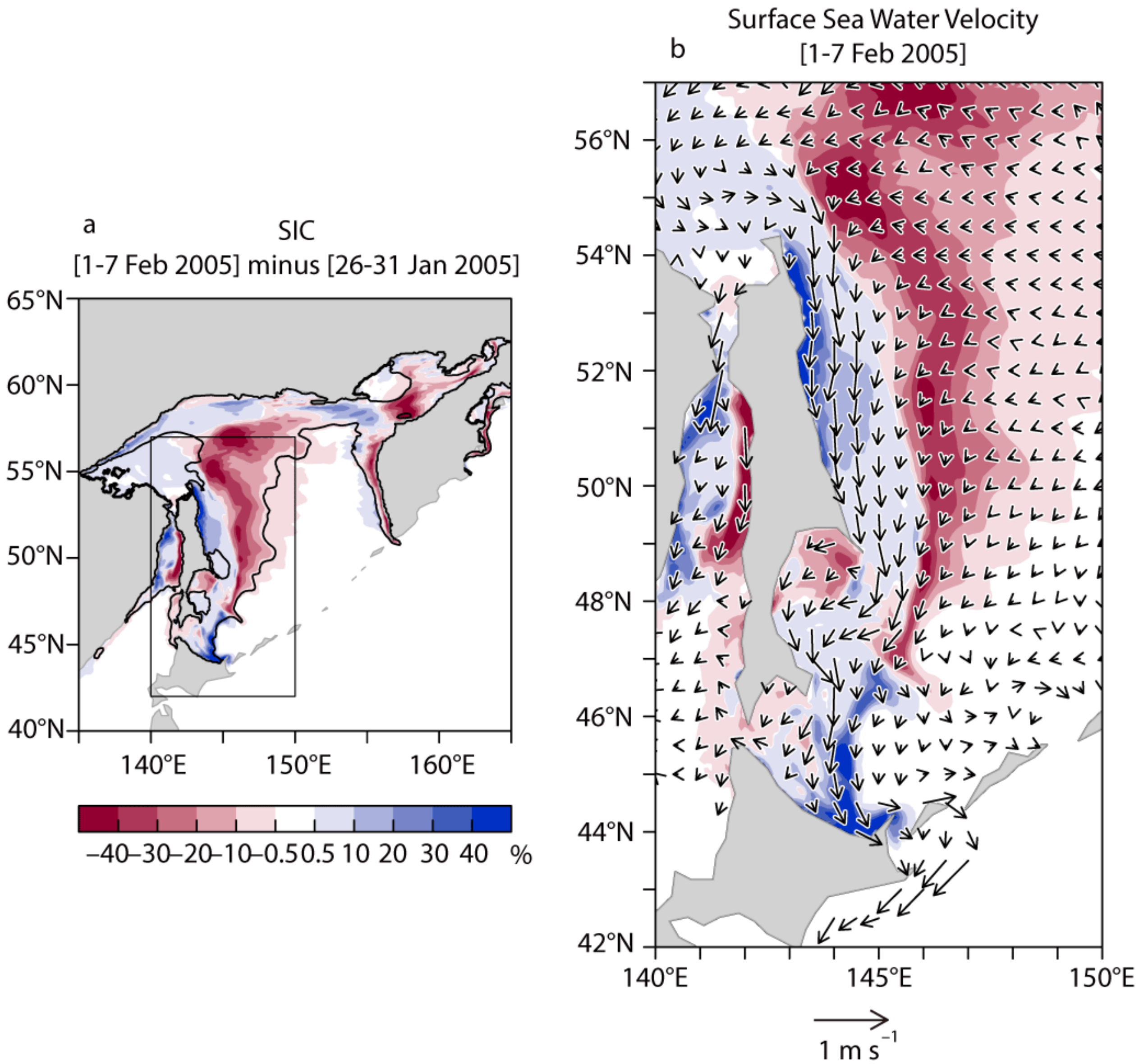

Fig. 3 SIC in the Okhotsk Sea in the example case of early February 2005. (a) SIC anomaly (shading; %) during February 1–7 minus January 26–31, 2005. Contours indicate SIC (5% and 90%) during January 26–31, 2005. Black rectangle indicates the domain examined in b. (b) Similar to (a) but with surface (0.5 m depth) sea water velocity (vector; m s^{-1}) during February 1–7, 2005.

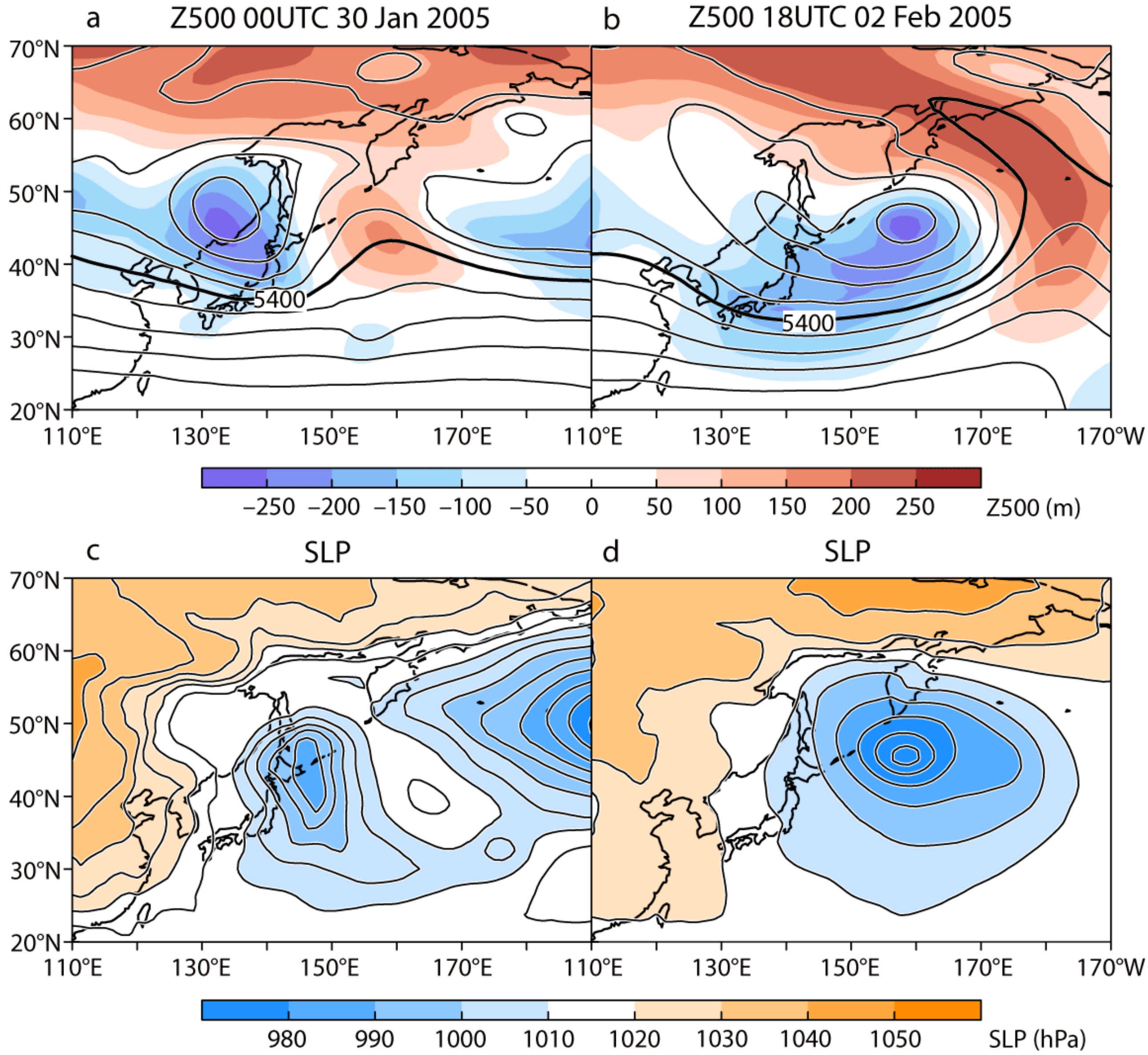

Fig. 4 Geopotential height at 500 hPa (Z500; m) and sea level pressure (SLP; hPa) in the example case of early February 2005. (a) Contours indicate Z500 at 00 UTC on January 30 and (b) at 18 UTC on February 2, 2005. Shading represents Z500 anomaly relative to its climatology (1991–2020). (c) Contours and shading indicate SLP at 00 UTC on January 30, and (d) at 18 UTC on February 2, 2005.

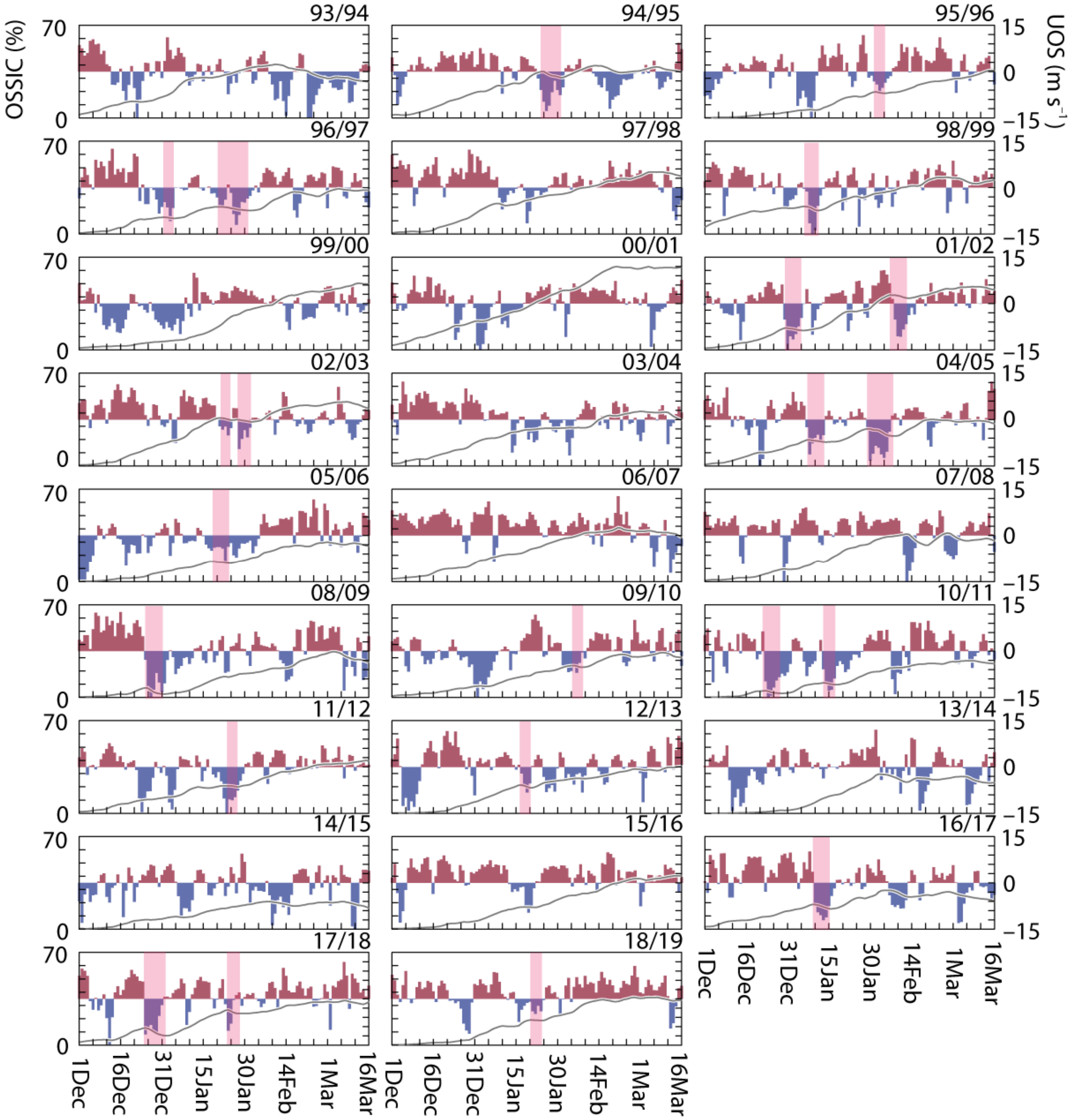

Fig. 5 Time series of OSSIC and UOS between December 1 and March 16 in 26 winters (from 1993/94 to 2018/19). The horizontal axis ranges for the leap years (1996, 2000, 2004, 2008, 2012, and 2016) are from December 1 to March 15. Gray lines indicate OSSIC (%). Red and blue shading represents positive (westerly) and negative (easterly) UOS (m s^{-1}), respectively, determined as 925 hPa zonal wind averaged over 47.6°–59.0°N, 142.3°–155.1°E (Fig. 1). Shading in light magenta indicates sea-ice reduction events (REs).

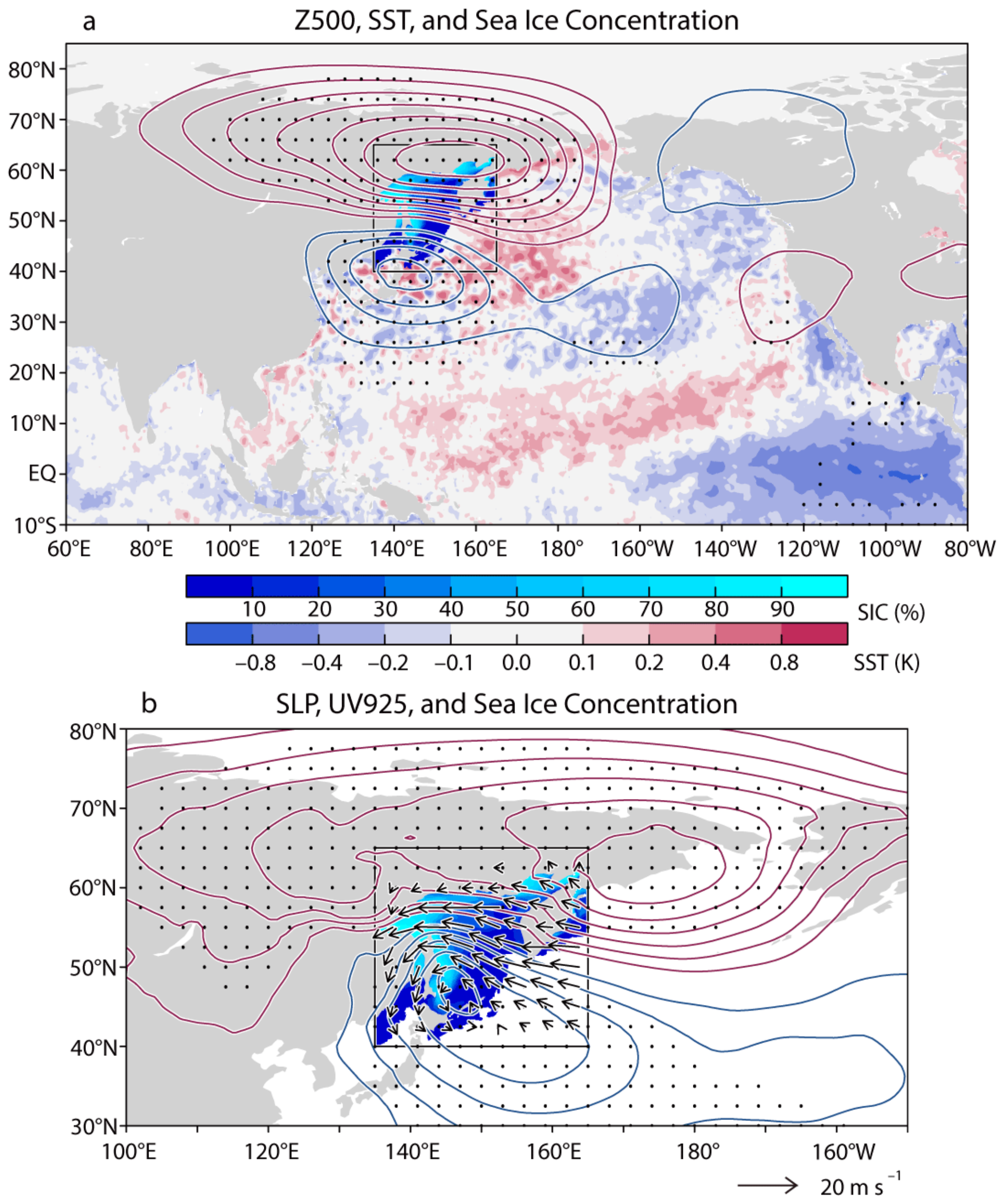

Fig. 6 Composite Z500, SLP, and SIC in the Okhotsk Sea during periods of REs. (a) Red and blue contours indicate Z500 anomaly (±10, 20, 30, 40 and 50 m). Light blue-light red shading indicates sea surface temperature (SST; K) anomaly based on OISST version 2 (Reynolds et al. 2007). Blue-cyan shading in (a) and (b) indicates SIC in the Okhotsk Sea (%). (b) Red and blue contours indicate SLP anomaly (±0.5, 1.0, 1.5, 2.0, and 2.5 hPa). Vectors indicate horizontal wind anomaly (m s^{-1}) at 925 hPa. Stipples indicate areas with 95% statistical confidence of (a) the Z500 anomaly and (b) the SLP anomaly.

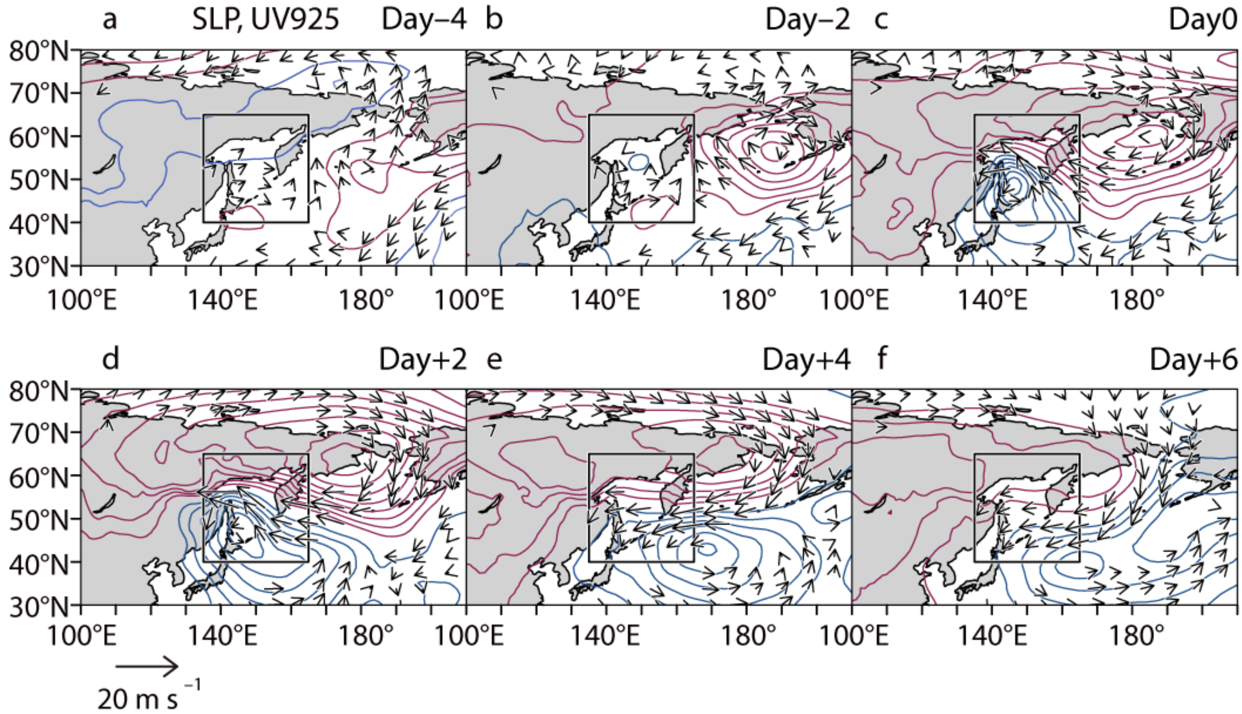

Fig. 7 Composite maps of SLP anomaly and horizontal wind anomaly at 925 hPa at (a) 4 days before the start of the REs (day –4), (b) day –2, (c) at the start (day 0), (d) 2 days after the start of REs (day +2), (e) day +4, and (f) day +6. Red (blue) contours indicate positive (negative) SLP anomaly (±0.5, 1.0, 1.5, 2.0, and 2.5 hPa). Vectors indicate horizontal wind anomaly (m s^{-1}) at 925 hPa.

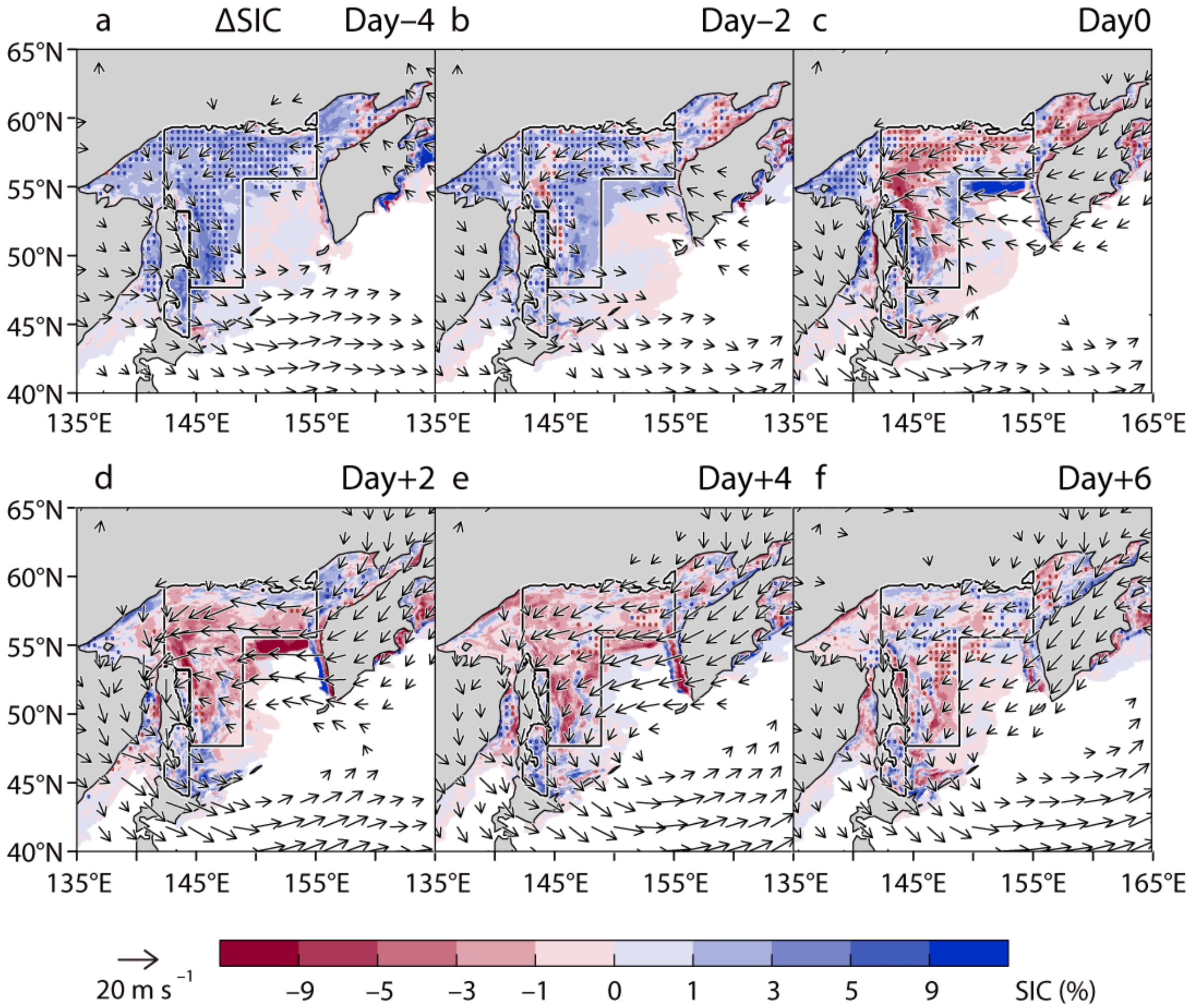

Fig. 8 Similar to Fig. 7, but composite maps of horizontal wind at 925 hPa over the Okhotsk Sea region. Shading indicates time tendency of SIC (% day^{-1}) in the Okhotsk Sea. Stipples indicate areas with 95% statistical confidence of the time tendency of SIC.

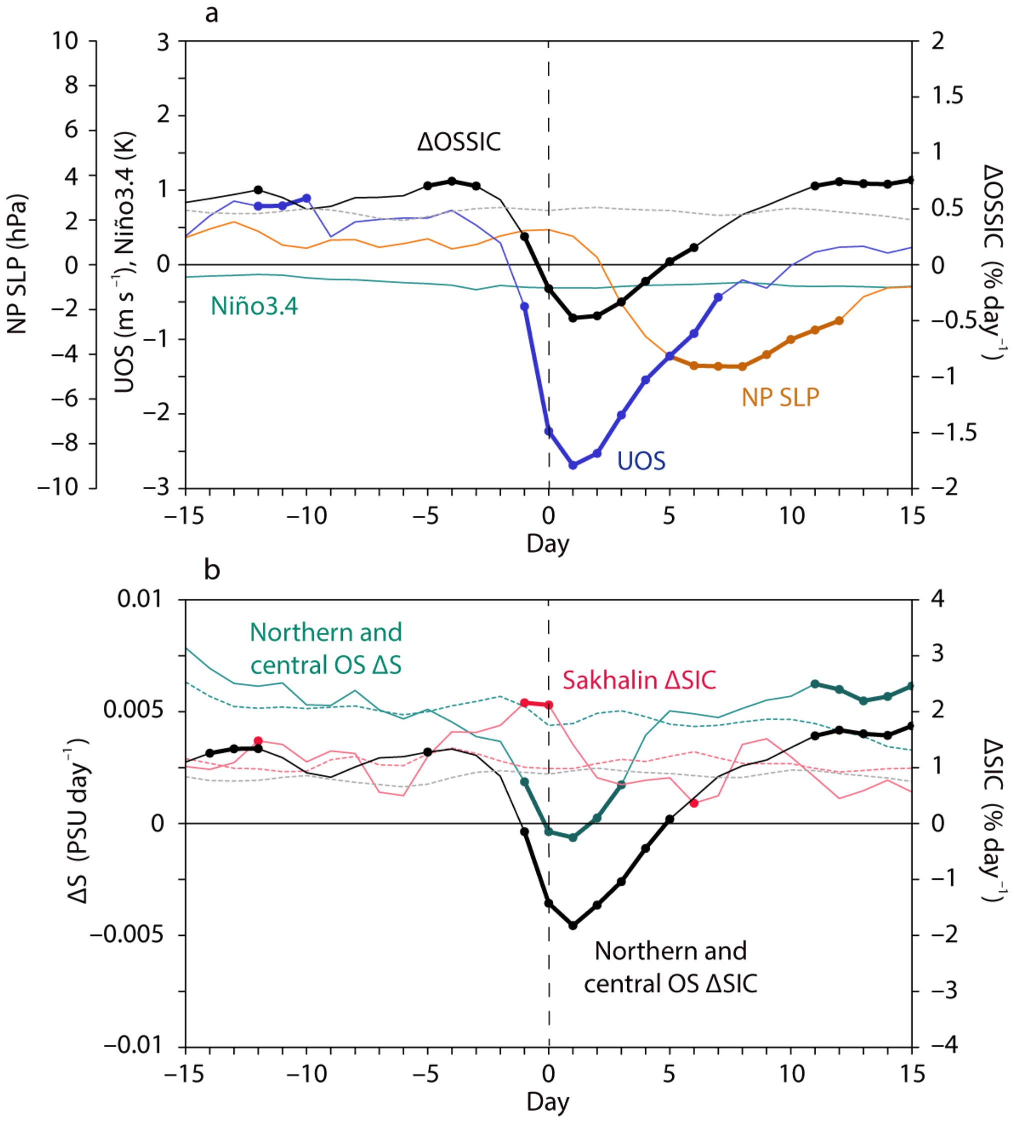

Fig. 9 Lagged composite between day –15 and day +15. (a) Black line indicates time tendency of OSSIC (ΔOSSIC, % day^{-1}). Gray dotted line indicates climatology of ΔOSSIC. Blue line represents UOS (m s^{-1}). Green line indicates SST anomaly over the Niño3.4 region (5°S–5°N, 170°–120°W; K). Brown line indicates SLP anomaly over the North Pacific Index region (30°–65°N, 160°E–140°W; hPa). Thick lines indicate >95% confidence levels. Black thick line indicates >95% confidence levels of ΔOSSIC anomaly relative to its climatology (black line minus gray dotted line). (b) Black and magenta lines indicate time tendency of SIC in the Sakhalin and Hokkaido coastal region (43.5°–53.2°N, 142.3°–144.4°E) and the northern and central OS region (47.6°–62.0°N, 142.3°–155.1°E),

respectively (Fig. 1). Green line indicates time tendency of sea surface salinity (PSU) in the northern and central OS region. Thick lines indicate >95% confidence levels of ΔSIC anomaly relative to the climatology (dotted lines).